Desalination and Water Treatment
www.deswater.com

doi: 10.5004/dwt.2022.28534

265 (2022) 48–56
July

Influence of graphene oxide with different sizes or layers on polyamide thin-film nanocomposite membranes

Meng Du[a], Yicheng Cao[a], Yilin Li[a], Peng Zhang[b], Yi Wei[a,b,*], Xueli Gao[c,*], Bo Wang[a]

[a]*Engineering Research Center of Fine Particle Pollution Control Technology and Equipment, College of Earth and Environmental Sciences, Lanzhou University, Lanzhou 730000, China, Tel. +86 13012488897; email: weiyi@lzu.edu.cn (Y. Wei)*
[b]*Key Laboratory for Resources Utilization Technology of Unconventional Water of Gansu Province, Lanzhou, Gansu, 730000, China*
[c]*Key Laboratory of Marine Chemistry Theory and Technology, Ministry of Education, Ocean University of China, Qingdao, Shandong, 266100, China, Tel. +86 13805326028; email: gxl_ouc@126.com (X. Gao)*

Received 7 December 2021; Accepted 25 April 2022

ABSTRACT

The chemical and physical properties of graphene oxide (GO) would affect the performance of thin-film nanocomposite (TFN) membrane. In this study, the effects of size and layer number of GO on TFN membranes were studied. The larger the size of nanosheets, the more obvious the modification effect on the surface morphology of the TFN membrane, and the better the chlorine resistance of the TFN membrane. As the size of GO becomes smaller, the rejection and flux of TFN membrane are better. The decrease of GO' size could eliminate the phenomenon of flux perk and reduce the decrease of rejection of TFN membranes. And also, because of fewer defects and more lamellar channels, TFN membrane modified with multilayered GO has a higher rejection than GO-TFN membrane when the flux is similar. These results will be helpful to understand the separation mechanism of GO-TFN membrane and optimize the structure of functional layer.

Keywords: Graphene oxide; Thin-film nanocomposite membrane; Reverse osmosis; Polyamide; Multilayered graphene oxide

1. Introduction

In order to mitigate the global water crisis, the use of desalination technology is becoming increasingly widespread. Because of high energy efficiency, reverse osmosis (RO) technology has been the most popular desalination technology [1,2]. Polyamide (PA) thin-film composite (TFC) membrane, the major RO membrane, has already occupied most of the market share. Up to now, different kinds of nanomaterials, for instance, zeolite [3], carbon nanotube [4] and titanium dioxide [5] have been applied to modify thin-film nanocomposite (TFN) membranes to enhance the performance of PA membranes [6].

Compared with the above additives, graphene oxide (GO), a two-dimensional nanomaterial, delivers more robust chargeability, higher hydrophilicity and better dispersibility with a great many oxygen-containing functional groups [7–13]. These properties make GO suitable as a modified material for TFN membranes. Whether adding GO to the aqueous solution or the n-hexane solution, the flux of TFN membranes can be improved [7,8,10]. Meanwhile, the PA active layer's thickness and roughness can also be regulated. In many studies, the flux of GO-TFN membrane had a maximum at a certain GO addition level [7,8,10,14,15]. If more GO was added, the flux of TFN membrane would increase considerably, with a significant decrease of salt

* Corresponding authors.

rejection. When the concentration of GO in the aqueous solution was 0.3%, the salt rejection of TFN membrane to NaCl (2,000 ppm) is reduced to 30% [9]. The improved permeability of GO-TFN membrane was associated with enhanced hydrophilicity and more nanochannels. The increase in flux at high GO concentration may be attributed to the defects formed from GO sheets or aggregations [9], which would result in a decline of salt rejection. In order to solve this problem, some researchers have functionalized GO to reduce the effect of agglomeration [16]. In addition, the chlorine resistance of GO modified TFN membrane was also improved [8,17]. The chlorine resistance of polyamide membrane can also be improved by using GO to modify the substrate [18]. The hydrogen bonding between GO and PA may prevent chlorine from replacing amidic hydrogen [19]. Due to its outstanding chemical stability, GO can also act as a physical barrier to active chlorine [20]. A large number of hydroxyl and carboxyl groups of GO may take the place of amide bonds to react with active chlorine [21]. The chlorine resistance of polyamide membrane can often be improved by using various nanomaterials [22,23]. The size of GO nanosheets may be one of the important factors affecting the chlorine resistance of GO-TFN membrane. And also, the size of GO nanosheets would affect the dimension of defects and the morphology of aggregates, which would affect the separation performance of GO-TFN membrane. In order to retain nanochannels and reduce the number of defect channels, multilayered GO may be a good choice. Multilayered GO, with lamellar nanochannels for the passageway of water molecules [23], could reduce the number of defects and introduce layered nanochannels into the separation layer for water permeation. Therefore, the properties of GO nanosheets, including size and layer number, are necessary to study for understanding the performance improvement of GO-TFN membranes.

In this paper, we used GO with different sizes prepared by ultrasonic crushing or GO with different layers prepared by the assembly-crosslink-exfoliation method as an additive to modify the PA membrane. The influence mechanism of GO with different sizes and layers on the desalination performance of GO-TFN membrane was discussed. And, the mechanism of chlorine resistance improvement of GO-TFN membrane, modified by GO with different sizes, was also discussed.

2. Material and methods

2.1. Materials

Expandable graphite was brought from Qingdao Laixi Nanshu Fada Graphite Co., China. H_2SO_4 (95 wt.%, AR) and HCl (37 wt.%, AR) were purchased from Beijing Chemical Works, China. H_2O_2 (30 wt.%, AR) was obtained by Tianjin Basf. $KMnO_4$ and NaCl (AR) were provided from Sinopharm Chemical Reagent Co., Ltd., China. Ethylenediamine (EDA), m-Phenylenediamine (MPD), trimesoyl chloride (TMC), triethylamine (TEA), camphorsulfonic acid (CSA) and n-Hexane were purchased from Aladdin Industrial Co. Polyethersulfone (PES) support with 50 K Daltons molecular weight cut-off (MWCO) was brought from Shandong Zhaojin Motian Co., Ltd., China. Dialysis bag (MWCO: 8,000–14,000) was bought from Huacheng Yimei Technology Co., Ltd., China. All water in the experiment was deionized (DI) water (resistivity = 18 MΩ/cm).

2.2. Methods

2.2.1. Preparation of GO with different size

GO was prepared by a modified Hummers method [25], where expandable graphite powder was oxidized in a mixture of concentrated H_2SO_4 and $KMnO_4$ below 5°C, heating the temperature of the mixture slowly up to 30°C–40°C and maintaining this temperature for 2.5 h. DI water was added slowly until no purple smoke appeared. Then, the resulting mixture was diluted and heated up to 95°C for 15 min. A large amount of water was added to terminate the reaction. After natural cooling, hydrogen peroxide was added and the color of the suspension liquid changed from brown to golden yellow. The mixture was then washed with 10% hydrochloric acid. Finally, graphite oxide was obtained by filtration and washing several times until the pH value was stable. Graphite oxide was vacuum-dried under 40°C.

GO solution, which called GO1, was prepared by ultrasonic exfoliation (in ultrasonic cell grinder, 48.75 W, 80 min) and centrifugation (8,000 rpm, 10 min). GO with smaller size were prepared by additional ultrasonic crushing in ultrasonic cell grinder with different ultrasonic power (162.5 W, 40 min for GO2 and 325 W, 40 min for GO3).

2.2.2. Preparation of multi-layered GO

EDA (300 mg) was added in to GO3 solution (100 mL, 0.1 mg/mL). After fully stirring, the mixture was filtrated through the ultrafiltration membrane by the self-designed membrane cell. When the surface of the self-assembly EDA-GO layer had no visible water, the membrane cell was sealed and placed at 60°C for thermal crosslinking for 2 h. Then, the cross-linked self-assembly GO membrane was treated by ultrasonic (162.5 W, 60 min) in water. At last, centrifugation (4,000 rpm, 10 min) and dialysis were used to obtain multi-layered graphene oxide (MGO) solution.

2.2.3. Preparation of TFN membrane

On the PES substrate's top surface, the TFC membranes and TFN membranes with GO and MGO were prepared by interfacial polymerization. The PES substrate was soaked in a 2.0 wt.% MPD water solution containing additives (camphor sulfonic 2.3 wt.%, sodium dodecyl sulfate 0.1 wt.%, triethylamine 1.1 wt.% and a certain amount of GO) for 5 min. Unnecessary solution on the surface was blown away by nitrogen purging. Then, the prepared layer was immersed in the 0.1 wt.% of TMC-hexane solution for 30 s. After removing the surplus hexane solution, the obtained TFN membrane was heat-treated at 80°C for 5 min. All prepared membrane samples were stored in DI water until further testing.

2.3. Characterization of GO-based materials

The GO nanosheets' size was characterized by atomic force microscopy (AFM, Veeco Multimode-V microscope)

and laser particle sizer (Zetasizer Nano ZS). A drop of GO solution was dropped onto a mica sheet and characterized after solvent evaporation. The GO-based materials' functional groups were characterized by Fourier-transform infrared spectroscopy (FTIR, Bruker Tensor 27). The d-spacing or thickness of nanosheets was characterized by AFM and X-ray diffraction (XRD, D8 ADVANCE). The XRD samples were multi-layered films prepared by self-assembly method.

2.3.1. Characterization of TFN membrane

The topography of TFN membranes was visualized by scanning electron microscopy (SEM, Hitachi S4800). The TFN membranes' roughness was analyzed by AFM. The tapping mode was used in AFM characterization. The cross-section samples of TFN membranes were prepared by fracturing in liquid nitrogen. The SEM samples were sputtered with nanogold before observation. A CA analyzer (Kruss DSA100) was used to measure the static contact angles of TFN membranes. The CA values were recorded when the water drip stayed on the membrane for 3 s.

2.3.2. Evaluation of TFN membrane

A cross-flow device was used to measure the separation performance of the TFN membrane. All the membrane samples were pressurized at 2.0 MPa until the flux was constant. The NaCl solution (2000 ppm) was used to evaluate salt rejection. Rejection (R) and salt water flux (F) were calculated using the following two equations respectively,

$$R = \left(1 - \frac{C_p}{C_f}\right) \times 100\% \quad (1)$$

where C_p and C_f were the salt concentration of permeated and feed solutions, respectively,

$$F = \frac{Q}{A} \quad (2)$$

where Q (L/h) represented the total volume of water passing through the TFN membrane per hour, A (m^2) was the effective membrane area. The salt concentration was measured by using the electrical conductivity meter (Leici, DDS-307A).

The TFN membranes' chlorine resistance was evaluated using the following method. The membrane samples were soaked in sodium hypochlorite solution with active chlorine concentration of 2,000 ppm for 2 h. After that, all samples were washed with DI water. Next, the water flux and the salt rejection membrane were evaluated in cross-flow device.

2.3.3. Characterization of GO aggregation

The GO aggregation was obtained by filtration. MPD solution containing GO with different size was filtrated through PES membrane and washed with deionized water for 5 times. The filtrate was characterized by FTIR after drying. The FTIR spectrums of GO with different size are used as the comparison data.

3. Results and discussion

3.1. Properties of GO-based materials

As seen in Fig. 1, different ultrasonic crushing can result in various sizes of GO nanosheets. Particle size analysis (Fig. 1d) also shows that GO with different sizes can be prepared by crushing power settings. After exfoliation, the size of GO1 is in the range of hundreds of nanometers. When high-power ultrasonic crushing is performed, the size of nanosheets (GO2 and GO3) is significantly reduced and decreases with increasing crushing power. As seen in Fig. 1d, the size of GO2 nanosheets is mainly distributed in two intervals. This indicates that ultrasonic treatment with the power of 162.5 W for 40 min is not enough to crush all the nanosheets. When the ultrasonic power was increased to 325 W, the size of nanosheets is below 20 nm.

The layer number of MGO was confirmed by AFM characterization. Fig. 2a shows the height curve of MGO nanosheets. As can be seen from the MGO nanosheets' thickness, the layer number of MGO is 2–4. Since EDA was used as an interlayered cross-linker in the preparation of MGO, the occurrence of the crossing reaction was confirmed using FTIR. The FTIR spectra of GO and MGO are illustrated in Fig. 2b. The out-of-plane blending vibration of N–H near 800 cm^{-1} shows that the crosslinking of GO by EDA is successful. Meanwhile, since the EDA solution is alkaline, GO would have a certain degree of reduction. The intensity of peaks corresponding to the oxygen-containing functional groups on the MGO spectrum is significantly reduced.

3.2. Influence of nanosheets' size on the separation performance of TFN membranes

As seen in Fig. 3, the addition of large-sized GO (GO1) has a pronounced influence on the surface morphology of TFN membranes. With the increase of the content of GO1 in aqueous solution, many continuous flat structures appear on the surface of TFN membranes. When the content of GO1 is 0.1%, the peak-valley structure on the surface of TFN membrane almost disappears (Fig. 3d1). Fig. 3 also shows the cross-section of GO1-TFN membranes, demonstrating that the thickness of the PA activity layer of TFN membrane declines significantly when the content of GO1 is 0.05% and 0.1%. The presence of GO nanosheets in aqueous solution affects the mass transfer process of interfacial polymerization, resulting in a change in the morphology of PA desalination layer. The AFM characterization results (Table 1) also show that the TFN membranes' roughness gradually decreases with the addition of GO1, because the peak-valley structure is the main reason for the increase of roughness. Moreover, as seen in Table 1, the contact angle decreases slightly with the increased flatness. Another reason for the decrease of contact angle is the addition of hydrophilic GO.

As seen in Fig. 3e, when the concentration of GO1 is lower than 0.05%, the flux increased with the addition of GO1. The flux decreases when more GO1 is added. This phenomenon is similar to other GO-TFN studies [8,10,14,15]. The space between GO nanosheet and PA can act as water channels. And a great many oxygen-containing functional groups on GO nanosheets give TFN membranes

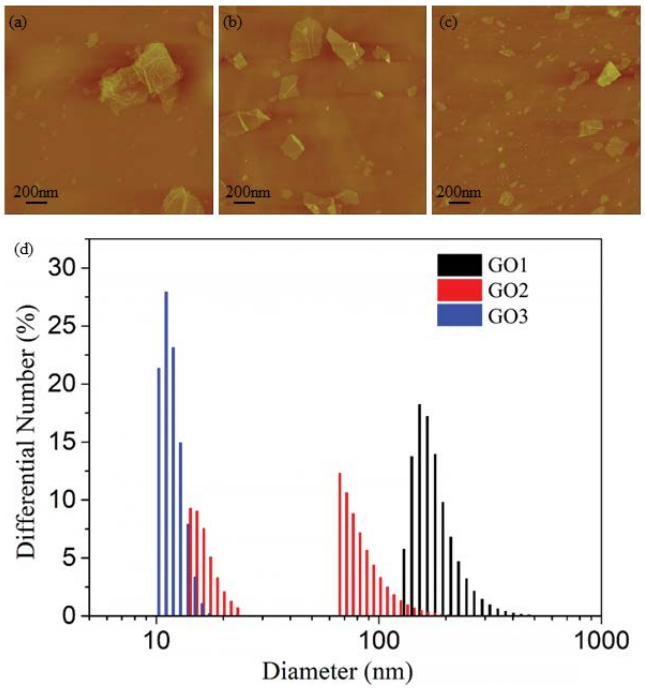

Fig. 1. (a–c) AFM images of GO nanosheets with different size: (a) GO1, (b) GO2 and (c) GO3. (d) Size distributions of GO1, GO2 and GO3 nanosheets.

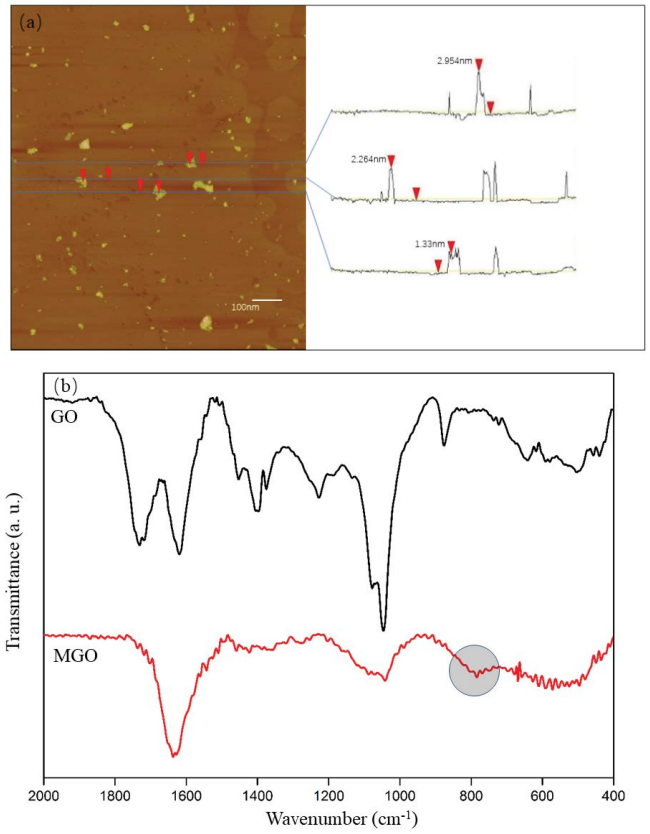

Fig. 2. (a) AFM image and the height curve of MGO nanosheets and (b) FTIR spectra of GO and MGO.

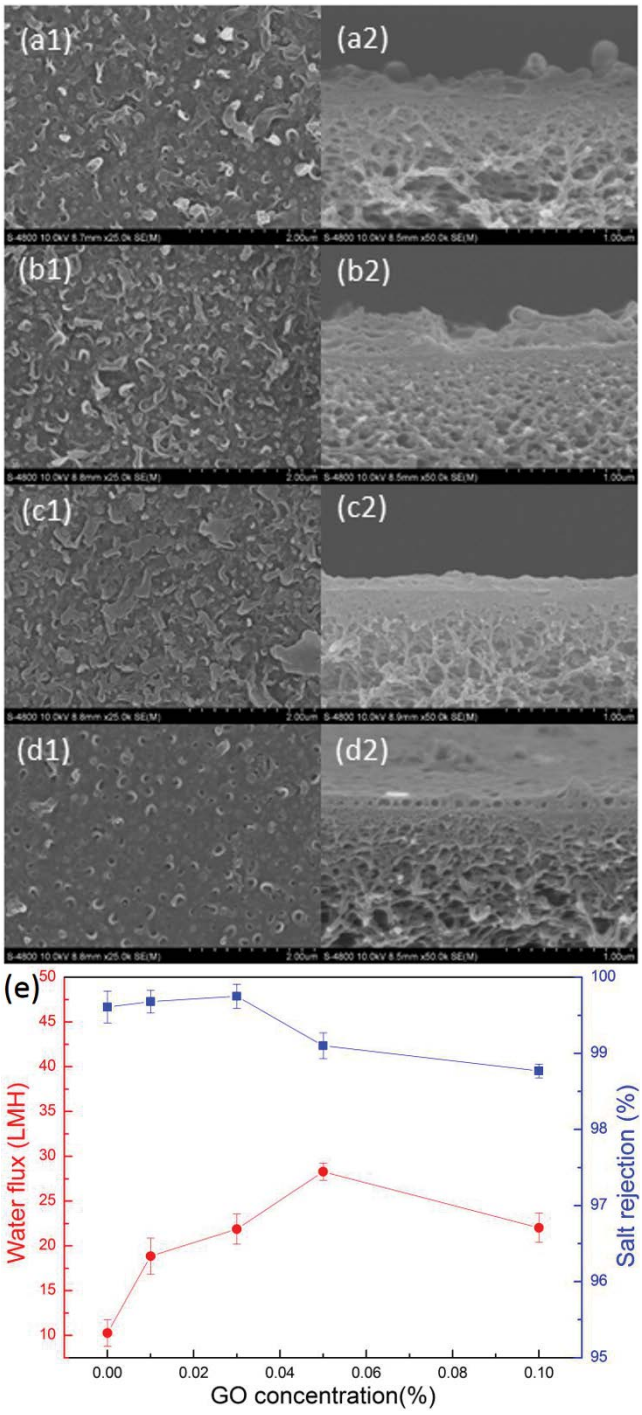

Fig. 3. SEM images of surface and cross-section of PA membranes modified with GO1 nanosheets. Concentration of GO1 in aqueous solutions: (a) 0.01%, (b) 0.03%, (c) 0.05%, (d) 0.1%. (e) Fluxes and salt rejections as two functions of the concentration of GO1.

better hydrophilicity. GO nanosheets can also affect the mass transfer process of interfacial polymerization, resulting in an increased free volume and thinner desalination layer [26,27]. These reasons lead to the increase of water flux. From Fig. 3d1, it can be inferred from the change of

surface morphology that the peak-valley structure almost disappears. The flat surface will reduce the comparative area, which will reduce the permeability of membrane [28]. Another reason for the decrease of flux may be the reduced number of defective channels. Aggregation of GO reduces the number of nanosheets that are present independently, thus reducing the number of introduced passageways.

The salt rejection drops below 99% when the GO1 concentration increases to 0.1%. The aggregation caused by high concentration of GO1 can form large-sized defects in TFN membrane, which can increase the penetration of ions. Therefore, GO1 with a high concentration in PA layer results in the decrease of flux and salt rejection simultaneously.

When the size of GO nanosheets is reduced, the effects of GO on the morphology and performance of GO-TFN membranes have changed. Fig. 4 shows the SEM images of GO2-TFN membranes' surface and cross-section. Compared with Fig. 3c1, there is no flat sheet structure in Fig. 4c1. Furthermore, as seen in Fig. 4d2 and Fig. 3d2, the smoothness of GO2-TFN (0.1%) membrane is lower than the smoothness of GO1-TFN (0.1%). This phenomenon manifests that the decrease in size of GO nanosheets slows down the hindrance of nanosheets on the mass transfer process of interfacial polymerization. However, as seen in Fig. 4d1, high concentration of GO2 also causes the loss of peak-valley structure. Comparing the cross-section images of Figs. 3 and 4, the effect of GO2 on the thickness of the PA layer is not as obvious as GO1. Table 2 illustrates the roughness and CA values of GO2-TFN membranes. The roughness of GO2-TFN membranes changes less than that of GO1-TFN membranes. The difference between the effects of GO1 and GO2 on the hydrophilicity of TFN membranes is not evident on the data of CA value, indicating that the oxygen-containing functional groups are still effective for improving the hydrophilicity of surface, although the size of GO nanosheets is reduced.

Fig. 4e shows the GO2-TFN membranes' flux and salt rejection. Interestingly, the flux of GO2-TFN membrane increases along with the concentration of GO2, while the decline of salt rejection is not apparent. Due to the reduced size of GO2, its dispersibility is improved so that the number of passageways in the PA layer introduced by GO2 nanosheets maintains a high level. And also, the improvement of hydrophilicity is still one of the reasons for the increase in flux. The decreased size of GO would also reduce the number and size of aggregations. Salt rejection of GO2-TFN membranes decreases with increasing GO2 concentration, but it remains above 99%. The decreasing rate of salt rejection is not obvious, indicating that the size of the defects introduced by GO2 is not large.

As the size of GO nanosheets continues to decrease, GO3's influence on the surface morphology of TFN membrane is not as pronounced as that of GO1 and GO2. Fig. 5 shows the GO3-TFN membranes' SEM images. GO3-TFN membrane has more ridge-and-valley structure than GO2-TFN membrane and GO1-TFN membrane when the concentration of GO is 0.1%. Moreover, the roughness values of GO3-TFN membranes are higher than GO1-TFN and GO2-TFN membranes (Table 3). This phenomenon indicates that smaller GO nanosheets have less effect on the mass transfer process of interfacial polymerization and impose less hindrance to the diffusion of monomers as well.

Fig. 5e shows that the separation performance of GO3-TFN membranes is similar to that of GO2-TFN membranes. Additionally, as the concentration of GO is 0.1%, the salt rejection of GO3-TFN membranes is slightly higher than it of GO2-TFN membranes.

In order to characterize the occurrence of reaction between GO and MPD, we filtered and washed the aqueous solution including GO and MPD only and the filtration product was characterized by FTIR after vacuum drying at room temperature. As seen in Fig. 6b, the absorption peaks associated with the C–N stretching vibration near 1,500 cm^{-1} and the N–H blending vibration near 800 cm^{-1} show that the reaction between GO and MPD can be carried out during the interfacial polymerization. The reaction between epoxy and amino can promote the occurrence of agglomeration. Smaller nanosheets form relatively small aggregation and reduce the probability of the formation of large-sized defects, which is one of the reasons for the decline of salt rejection. And also, the effect of small nanosheets on the diffusion of monomers is relatively small, which also leads to a high level of desalination performance.

Table 2
Surface roughness and static contact angle of PA membranes modified with GO2 nanosheets

Concentration	Rms (nm)	Ra (nm)	CA (°)
0.01%	33.210	25.395	58.16
0.03%	32.027	23.984	55.24
0.05%	27.396	20.586	52.06
0.1%	24.095	18.27	47.93

Table 1
Surface roughness and static contact angle of PA membranes modified with GO1 nanosheets

Concentration	Rms (nm)	Ra (nm)	CA (°)
0.01%	33.566	25.743	59.23
0.03%	30.150	22.570	55.18
0.05%	25.602	18.091	52.35
0.1%	23.909	18.340	48.52

Table 3
Surface roughness and static contact angle of PA membranes modified with small GO nanosheets

Concentration	Rms (nm)	Ra (nm)	CA (°)
0.01%	32.323	24.073	57.03
0.03%	32.060	24.481	54.86
0.05%	31.451	23.251	51.67
0.1%	30.541	23.312	48.05

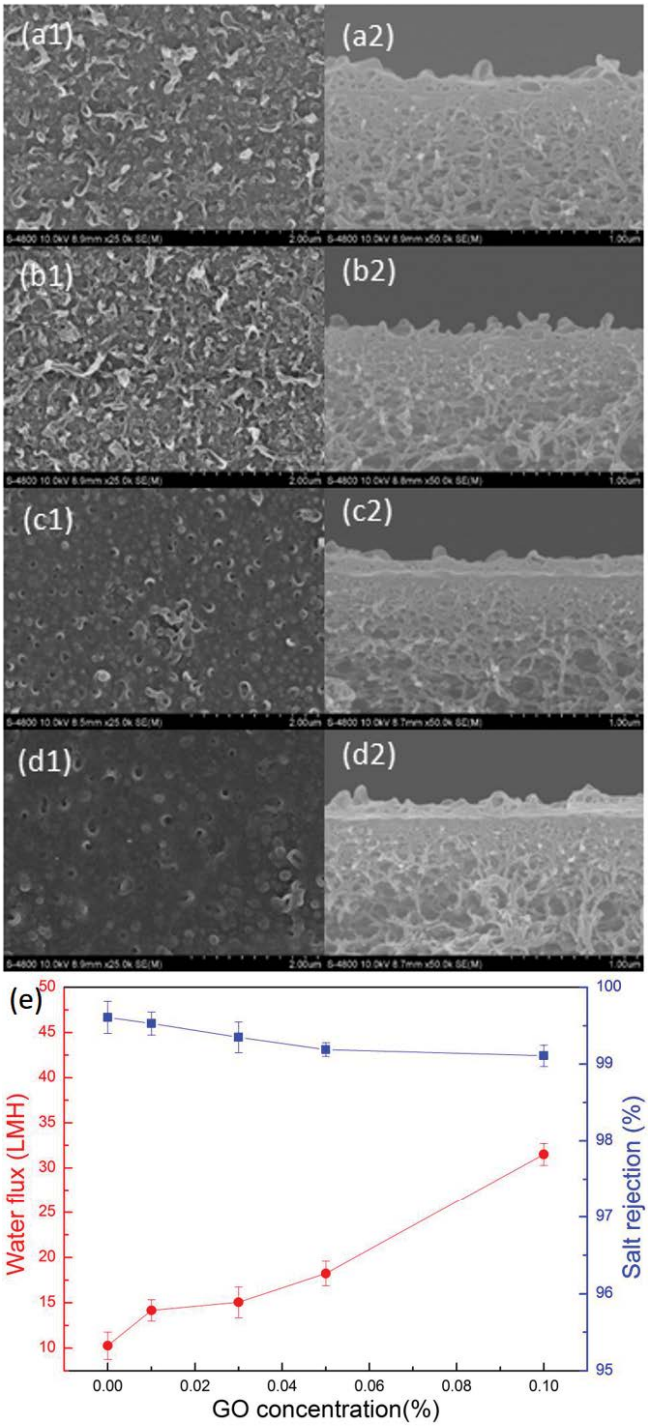

Fig. 4. SEM images of surface and cross-section of PA membranes modified with GO2 nanosheets. Concentration of GO2 in aqueous solutions: (a) 0.01%, (b) 0.03%, (c) 0.05%, (d) 0.1%. (e) Fluxes and salt rejections as two functions of the concentration of GO2.

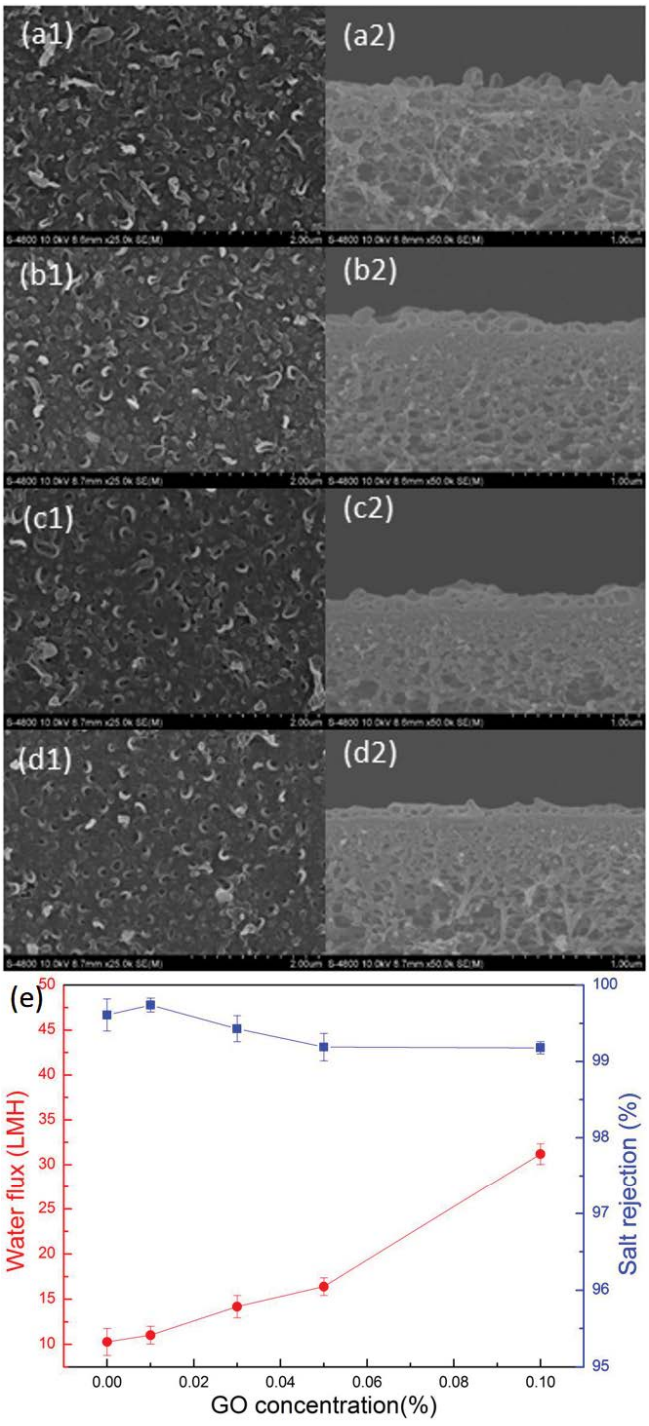

Fig. 5. SEM images of surface and cross-section of PA membranes modified with GO3 nanosheets. Concentration of GO3 in aqueous solutions: (a) 0.01%, (b) 0.03%, (c) 0.05%, (d) 0.1%. (e) Fluxes and salt rejections as two functions of the concentration of GO3.

3.3. Influence of nanosheets' size on the chlorine resistance of TFN membranes

So as to show the difference in chlorine resistance of TFN membranes more clearly, the change in salt rejection is converted into the change in flux of salt. Fig. 7 presents an analysis of the chlorine resistance of TFC and TFN membranes. The results clearly show that the salt permeation of TFC membranes increases by more than 400%,

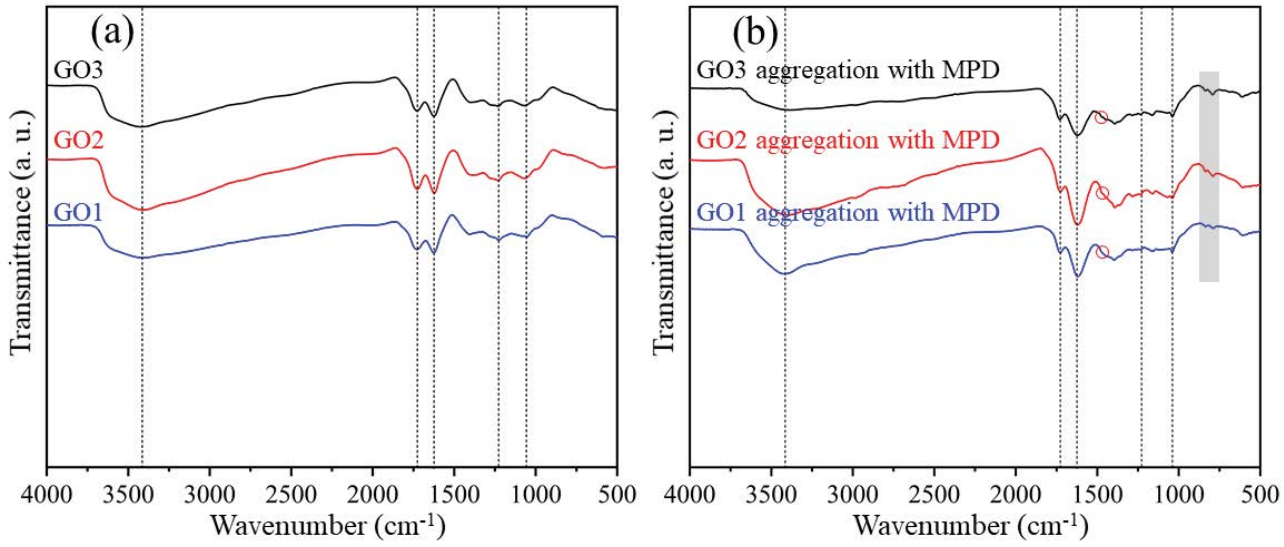

Fig. 6. FTIR spectra of (a) GO and (b) GO aggregation with MPD.

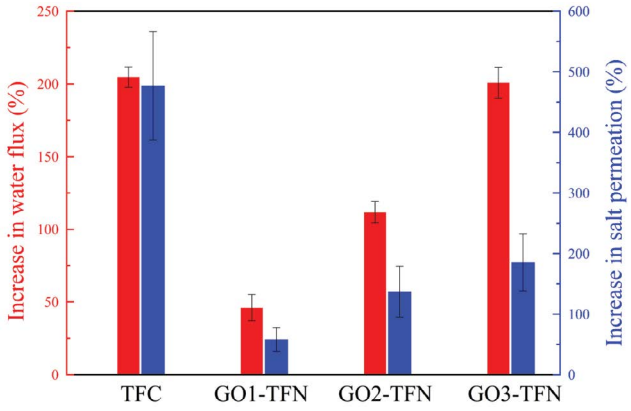

Fig. 7. The increase in water flux and salt permeation of TFC and TFN membranes after chlorinating treatment.

while the increase in salt permeation of TFN membranes is reduced to less than 200%. In the process of interfacial polymerization, we use nitrogen purging to remove excess aqueous solution. In this process, GO nanosheets have self-assembly behavior on the membrane surface. After the polyamide layer is formed, the two-dimensional plane of GO was parallel to the surface of the substrate membrane. When the polyamide membrane is chlorinated, the hypochlorite penetrates into the membrane and destroyed the amide bond. GO nanosheets can prevent the diffusion of active chlorine to a certain extent. At the same time, the interception ability of polyamide layer decreases after the degree of crosslinking decreases, but the existence of GO nanosheets will not significantly reduce the ion penetration resistance. In this case, large GO has a great impact on ion penetration, and the chlorine resistance is better. Larger GO nanosheets give TFN membranes better chlorine resistance, which indicates that the improved chlorine resistance of GO-TFN membranes is mainly due to physical hindrance of GO nanosheets.

3.4. Difference in performance of TFN membrane with single-layered GO and multi-layered GO

With the purpose of reducing the impact of aggregation and studying whether the layer number of GO will affect the performance of the TFN membrane, MGO was prepared and used to modify PA membrane. GO3 and MGO solutions with the same mass concentration were used to fabricate TFN membranes. As seen in Fig. 8, the surface morphologies of GO3-TFN and MGO-TFN membranes show a significant difference. The surface morphology of MGO-TFN membrane is nearly the same as the blank TFC membrane. Because at the same mass concentration, the number of nanosheets in MGO solution is less than that in GO3 solution. The decrease in the number of nanosheets results in almost no change in surface morphology of MGO-TFN membrane.

We used GO3 to prepare MGO, so that the main differences between GO3-TFN membrane and MGO-TFN membrane are the number of GO layers and nanosheets. Fig. 8g presents that MGO-TFN membrane has the higher salt rejection than GO3-TFN membrane. And also, GO3-TFN and MGO-TFN membranes have almost the same flux. Comparing with TFC membrane, GO3-TFN membrane has lower salt rejection and higher flux. The decrease of salt rejection is caused by defect channels. For MGO-TFN membrane, the layer spacing of MGO is too small for ions to pass through so that the increase of MGO layers will not produce the new ion channels. And also, fewer nanosheets lead to a decrease in the number of defects. Although the number of defect channels is reduced, the interlayer of MGO can also provide new water channels. So, compared with GO3-TFN membrane, MGO-TFN membrane has better desalination performance while keeping the permeability unchanged. Compared with GO3-TFN membranes, the improvement of MGO-TFN membranes on salt rejection can further explain the influence of aggregation on desalination performance.

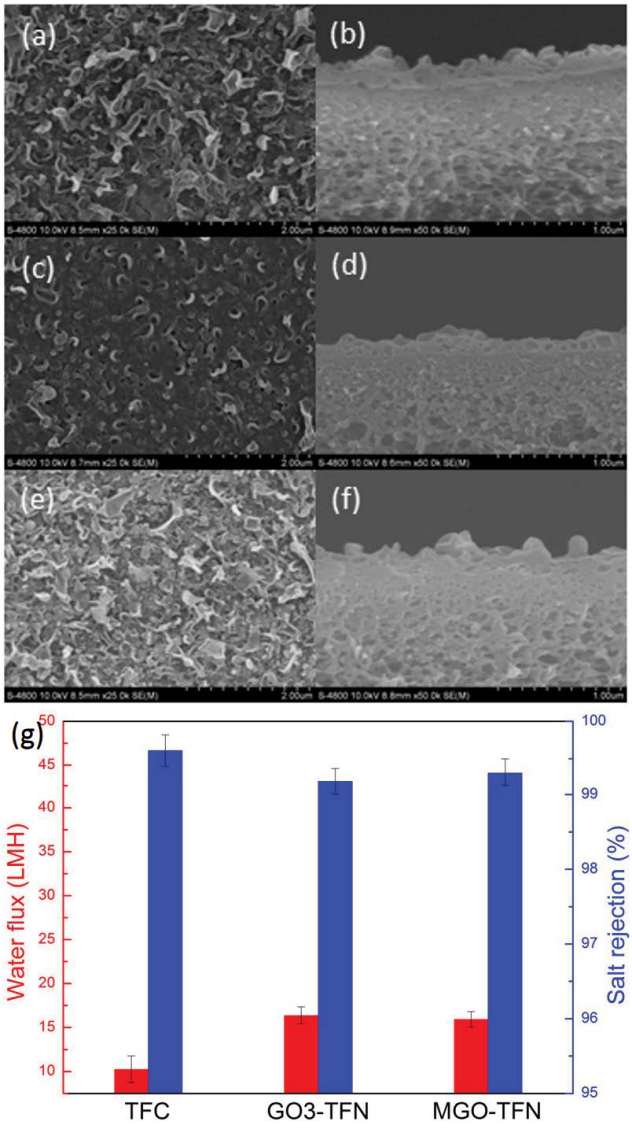

Fig. 8. SEM images of surface and cross-section of (a, b) blank TFC membrane, (c, d) GO3-TFN and (e, f) MGO-TFN membranes. (g) Flux and salt rejection of TFC, GO3-TFN and MGO-TFN membranes

4. Conclusions

In this study, GO with different sizes and layers were successfully used to modify PA membranes. Reducing the size of nanosheets can avoid the adverse effects of high concentration GO on water flux and salt rejection. Smaller nanosheets have less effect on monomer diffusion, and then have less effect on the peak valley structure of the membrane surface, which is very important to maintain the permeability. In addition, reducing the size of nanosheets helps to reduce the size of aggregates, which has a negative effect on the desalination performance. MGO can reduce the number of defect channels and introduce layered channels in PA layer. MGO-TFN membrane can obtain higher salt rejection while keeping the flux unchanged. It is an ideal strategy to introduce ideal water channels and reduce defect channels for improving the performance of GO-TFN membrane. Studying the effect of interlayer spacing with MGO on the performance of MGO-TFN membrane is of great significance in the future.

CRediT authorship contribution statement

M. D., Y. C. and Y. W. conceived the original idea and performed the experiments with the contribution of Y. L. The manuscript was written by Y. W. P. Zh., X. G. and B. W. provide funds and experimental sites. All authors have read the manuscript.

Acknowledgements

This work was supported by the National Key Research and Development Projects (2019YFD0900502), the Key Research & Development in Gansu Province (20YF8FA112), the Key Research Project of Shandong Province (2019JZZY010806), the Decentralized Sewage Treatment Technology Innovation Platform and the Young Taishan Scholars Program of Shandong Province.

References

[1] K.P. Lee, T.C. Arnot, D. Mattia, A review of reverse osmosis membrane materials for desalination—development to date and future potential, J. Membr. Sci., 370 (2011) 1–22.
[2] L.F. Greenlee, D.F. Lawler, B.D. Freeman, B. Marrot, P. Moulin, Reverse osmosis desalination: water sources, technology, and today's challenges, Water Res., 43 (2009) 2317–2348.
[3] L. Li, J. Dong, T.M. Nenoff, R. Lee, Desalination by reverse osmosis using MFI zeolite membranes, J. Membr. Sci., 243 (2004) 401–404.
[4] S.-M. Xue, Z.-L. Xu, Y.-J. Tang, C.-H. Ji, Polypiperazine-amide nanofiltration membrane modified by different functionalized multi-walled carbon nanotubes (MWCNTs), ACS Appl. Mater. Interfaces, 8 (2016) 19135–19144.
[5] M. Peyravi, M. Jahanshahi, A. Rahimpour, A. Javadi, S. Hajavi, Novel thin-film nanocomposite membranes incorporated with functionalized TiO_2 nanoparticles for organic solvent nanofiltration, Chem. Eng. J., 241 (2014) 155–166.
[6] X. Lu, M. Elimelech, Fabrication of desalination membranes by interfacial polymerization: history, current efforts, and future directions, Chem. Soc. Rev., 50 (2021) 6290–6307.
[7] H.-R. Chae, C.-H. Lee, P.-K. Park, I.-C. Kim, J.-H. Kim, Synergetic effect of graphene oxide nanosheets embedded in the active and support layers on the performance of thin-film composite membranes, J. Membr. Sci., 525 (2017) 99–106.
[8] H.-R. Chae, J. Lee, C.-H. Lee, I.-C. Kim, P.-K. Park, Graphene oxide-embedded thin-film composite reverse osmosis membrane with high flux, anti-biofouling, and chlorine resistance, J. Membr. Sci., 483 (2015) 128–135.
[9] L. He, L.F. Dumée, C. Feng, L. Velleman, R. Reis, F. She, W. Gao, L. Kong, Promoted water transport across graphene oxide–poly(amide) thin film composite membranes and their antibacterial activity, Desalination, 365 (2015) 126–135.
[10] M.E.A. Ali, L. Wang, X. Wang, X. Feng, Thin film composite membranes embedded with graphene oxide for water desalination, Desalination, 386 (2016) 67–76.
[11] H. Li, W. Shi, Q. Du, R. Zhou, H. Zhang, X. Qin, Improved separation and antifouling properties of thin-film composite nanofiltration membrane by the incorporation of cGO, Appl. Surf. Sci., 407 (2017) 260–275.
[12] Y. Si, E.T. Samulski, Synthesis of water soluble graphene, Nano Lett., 8 (2008) 1679–1682.

[13] J.I. Paredes, S. Villar-Rodil, A. Martínez-Alonso, J.M.D. Tascón, Graphene oxide dispersions in organic solvents, Langmuir, 24 (2008) 10560–10564.
[14] S. Xia, L. Yao, Y. Zhao, N. Li, Y. Zheng, Preparation of graphene oxide modified polyamide thin film composite membranes with improved hydrophilicity for natural organic matter removal, Chem. Eng. J., 280 (2015) 720–727.
[15] S. Bano, A. Mahmood, S.-J. Kim, K.-H. Lee, Graphene oxide modified polyamide nanofiltration membrane with improved flux and antifouling properties, J. Mater. Chem. A, 3 (2015) 2065–2071.
[16] F.-x. Kong, Z.-Y. Yang, L.-P. Yue, J.-f. Chen, C.-m. Guo, Nanofiltration membrane with substrate incorporated amine-functionalized graphene oxide for enhanced petrochemical wastewater and shale gas produced water desalination, Desalination, 517 (2021) 115246, doi: 10.1016/j.desal.2021.115246.
[17] F. Shao, X. Su, X. Shen, S. Ren, H. Wang, Z. Yi, C. Xu, L. Yu, L. Dong, Highly improved chlorine resistance of polyamide reverse membrane by grafting layers of graphene oxide, Sep. Purif. Technol., 254 (2021) 117586, doi: 10.1016/j.seppur.2020.117586.
[18] J. Zhang, S. Li, D. Ren, H. Li, X. Lv, L. Han, B. Su, Fabrication of ultra-smooth thin-film composite nanofiltration membrane with enhanced selectivity and permeability on interlayer of hybrid polyvinyl alcohol and graphene oxide, Sep. Purif. Technol., 268 (2021) 118649, doi: 10.1016/j.seppur.2021.118649.
[19] M. Abbaszadeh, D. Krizak, S. Kundu, Layer-by-layer assembly of graphene oxide nanoplatelets embedded desalination membranes with improved chlorine resistance, Desalination, 470 (2019) 114116, doi: 10.1016/j.desal.2019.114116.
[20] W. Choi, J. Choi, J. Bang, J.-H. Lee, Layer-by-layer assembly of graphene oxide nanosheets on polyamide membranes for durable reverse-osmosis applications, ACS Appl. Mater. Interfaces, 5 (2013) 12510–12519.
[21] C. Xu, F. Shao, Z. Yi, H. Dong, Q. Zhang, J. Yu, J. Feng, X. Wu, Q. Zhang, L. Yu, L. Dong, Highly chlorine resistance polyamide reverse osmosis membranes with oxidized graphitic carbon nitride by ontology doping method, Sep. Purif. Technol., 223 (2019) 178–185.
[22] S. Basu, M. Balakrishnan, Polyamide thin film composite membranes containing ZIF-8 for the separation of pharmaceutical compounds from aqueous streams, Sep. Purif. Technol., 179 (2017) 118–125.
[23] F. Asempour, S. Akbari, M.H. Kanani-Jazi, A. Atashgar, T. Matsuura, B. Kruczek, Chlorine-resistant TFN RO membranes containing modified poly(amidoamine) dendrimer-functionalized halloysite nanotubes, J. Membr. Sci., 623 (2021) 119039, doi: 10.1016/j.memsci.2020.119039.
[24] R.R. Nair, H.A. Wu, P.N. Jayaram, I.V. Grigorieva, A.K. Geim, Unimpeded permeation of water through helium-leak–tight graphene-based membranes, Science, 335 (2012) 442–444.
[25] W.S. Hummers Jr., R.E. Offeman, Preparation of graphitic oxide, J. Am. Chem. Soc., 208 (1958) 1334–1339.
[26] J. Yin, E.-S. Kim, J. Yang, B. Deng, Fabrication of a novel thin-film nanocomposite (TFN) membrane containing MCM-41 silica nanoparticles (NPs) for water purification, Procedia Eng., 44 (2012) 238–246.
[27] H. Wu, B. Tang, P. Wu, Optimizing polyamide thin film composite membrane covalently bonded with modified mesoporous silica nanoparticles, J. Membr. Sci., 428 (2013) 341–348.
[28] M. Hirose, H. Ito, Y. Kamiyama, Effect of skin layer surface structures on the flux behaviour of RO membranes, J. Membr. Sci., 121 (1996) 209–215.